Secrecy energy efficiency maximization in dual-metasurface-aided wireless networks

Fotock *et al.*
EURASIP Journal on Advances in Signal Processing (2025) 2025:24
https://doi.org/10.1186/s13634-025-01231-w

EURASIP Journal on Advances in Signal Processing

RESEARCH Open Access

Secrecy energy efficiency maximization in dual-metasurface-aided wireless networks

Robert Kuku Fotock[1], Agbotiname Lucky Imoize[2,3], Alessio Zappone[1*] and Ciro D'Elia[1]

*Correspondence:
alessio.zappone@unicas.it

[1] University of Cassino and Southern Lazio, Cassino, Italy
[2] Consorzio Nazionale Interuniversitario per le Telecomunicazioni, Parma, Italy
[3] Department of Electronic and Telecommunications, Politecnico di Torino, Torino, Italy

Abstract

This paper investigates the robust secure energy efficiency (SEE) maximization problem in a multiple-input single-output communication system enhanced by two reconfigurable metasurfaces in the presence of a single passive eavesdropper. One metasurface is placed in the near field of the transmit antenna array, forming a reconfigurable holographic beamforming structure. The second metasurface is placed in the environment between the transmitter and receiver, as a reconfigurable intelligent surface. The signal reaches the intended receivers both via a direct and through the two metasurfaces. In this context, we aim at maximizing the minimum SEE among all legitimate users under quality of service requirements, transmit power limitations, and reflection constraints. The resulting problem is non-convex, and we develop a novel algorithm based on alternating maximization, sequential fractional programming, and use of pricing techniques. Numerical results show that the proposed system architecture and radio resource allocation algorithms provide significant SEE gains over conventional alternatives.

Keywords: Reconfigurable holographic surfaces, Reconfigurable intelligent surfaces, Energy efficiency, Physical layer security, Resource allocation

1 Introduction

The use of metasurfaces is rapidly becoming one of the main candidate technologies for future 6G wireless networks [1–5]. Metasurfaces require simpler hardware, thus allowing the deployment of a larger number of electromagnetic elements than in traditional antenna arrays, while at the same time consuming less energy thanks to their analog operation, which dispenses with the use of analog-to-digital converters and other complex hardware components. Metasurfaces have the potential to meet the energy efficiency (EE) requirements of future 6G networks, significantly improving the energy efficiency of 5G technologies. In [6], it is argued that 5G technologies like massive multiple-input multiple-output (MIMO) provide much higher rate levels, but at the price of a power consumption that can be up to three times higher than legacy 4G technologies, mainly due to the large size of digital antenna arrays. As a result, the EE of 3rd Generation Partnership Project (3GPP) new radio deployments is estimated to be approximately four times larger than that of 3GPP long term evolution deployments. In this context, metasufaces can achieve a better compromise between deploying many

reflecting elements for high rate, while at the same time keeping the energy consumption at bay. It has been proposed to deploy metasurfaces both far from the wireless transceivers, to be used in a relay-like fashion, creating new propagation paths from the transmitter to the receiver, or in the immediate vicinity of the transceiver antennas, to allow for the use of fewer digital antennas. In the first case, metasurfaces are usually referred to reconfigurable intelligent surfaces (RISs), while, in the second case, the term reconfigurable holographic surfaces (RHS) or holographic beamforming is used. Moreover, metasurfaces can be both nearly-passive, i.e. no amplifier is equipped on the metasurface and the only energy that is required for their operation is that needed to operate the hardware components that enable the reconfiguration of the reflecting elements, or active, i.e. analog amplifiers are equipped on the metasurface, to combat the so-called double or multiplicative fading effect [7, 8]. Nevertheless, in both cases the metasurfaces operate only in the analog domain, thus not requiring any digital-to-analog conversion. It has been shown that, while active RISs can provide higher rates compared to their nearly-passive counterparts, their performance in terms of network EE strongly depends on the energy requirements to operate the analog amplifier, which is an additional source of power consumption that tends to reduce the energy efficiency of the network [9].

In addition to a dramatic increase of EE, future wireless networks will also be required to ensure the privacy of the communication data [10, 11]. Physical layer security is a technique that can be used in parallel to traditional cryptographic techniques, as an additional layer of security [12]. Compared to traditional cryptographic techniques, physical layer security is less complex because it does not require any dedicated cryptographic algorithm, leveraging only information-theoretic concepts [13, 14], with application in RIS-aided networks, too [15]. Motivated by these considerations, this work addresses both issues of EE and confidentiality by physical layer security, in a wireless network in which two metasurfaces are employed: an RHS deployed in the near-field of the transmit antenna array, and an RIS deployed in the far-field from both the transmitter and receivers.

1.1 Prior works

EE and physical layer security can be addressed jointly through the notion of secrecy energy efficiency (SEE), defined as the amount of bits that can be reliably and securely transmitted per Joule of consumed energy [16]. In the context of wireless networks aided by metasurfaces, the majority of studies focus either on the secrecy of the communication, without analyzing the EE, or on the EE, without studying the secrecy of the communication.

As for the secrecy aspect, in [17], the authors study the system secrecy outage probability of a RIS-aided non-orthogonal multiple access (NOMA) network. A RIS-aided NOMA-based network is also considered in [18], where the secrecy outage probability is analyzed. In [19], the secrecy outage and average rate of an RIS-aided network are evaluated considering a RIS with discrete phase shifts. The ergodic secrecy rate of an RIS-aided wireless network with multiple eavesdroppers is derived in [20], while the worst-case secrecy capacity maximization is addressed in [21], with reference to a NOMA-based system. In [22], the secrecy outage probability of an RIS-aided network is analyzed, whereas the secrecy rate of an RIS-aided network powered by wireless power

transfer is maximized in [23]. In [24], the secrecy rate of an RIS-aided network with space-ground communications is optimized. In [25], the secrecy rate of a multi-user RIS-aided wireless network is investigated.

As for the EE aspect, most studies do not consider the secrecy of the communication. In [26], an omnidirectional RIS is optimized to enhance the performance of vehicular networks, by minimizing the base station (BS) transmit power, subject to quality of service (QoS) constraints. In [27], an RIS-aided network is considered, and sum-rate maximization and power consumption minimization are tackled by optimizing the RIS reflection coefficients, and BS transmit powers. The tradeoff between fully connected and sub-connected architectures for active RISs is investigated in [28], with reference to a multiple-antenna system. The maximization of the network EE is carried out with respect to the RIS reflection coefficients and transmit beamforming. In [29], the EE of a multi-user RIS-aided MISO system is optimized with respect to the BS beamforming and the RIS reflection coefficients. The problem is tackled by means of the quadratic transform method for fractional problems [30]. A recent study in [31] considers a hybrid RIS with both nearly-passive and active elements and aims at optimizing the number of passive and active elements deployed to maximize the minimum among the ergodic energy efficiencies of the mobile users, considering a single-antenna BS. In [9], the EE of a multi-user wireless network is considered, and resource allocation algorithms are provided to optimize the RIS reflection coefficients, the users transmit powers, and BS receive filters. In [32], a satellite communication in the presence of an eavesdropper is considered, in which an active RIS with local reflection capabilities is used to boost the received power. The minimum of the mobile users' SEEs is maximized with respect to the RIS reflection coefficients and transmit beamforming by an alternating maximization technique, assuming a bounded error model for the channel between the RIS and the eavesdropper.

The SEE of RIS-based networks is considered in fewer works. In [33], the optimization of the SEE of an RIS-aided network is conducted using deep reinforcement learning. The work [34] employs alternating maximization and sequential programming to maximize the SEE of a multi-user network. Similarly, the authors of [35] employ a blend of sequential programming and alternating optimization to optimize the minimum SEE of a multi-user network. However, these last works also focus on nearly-passive RISs without addressing the use of active RISs. In [36], it is shown that RISs can be used to provide secrecy and user authentication in visible light communication systems.

1.2 Contributions

This work considers the downlink of a multiple-input single-output (MISO) communication system where the transmitter communicates with multiple legitimate users through two metasurfaces, one RHS co-located with the BS antenna array and an RIS placed in the environment between the BS and the mobile users. A passive eavesdropper is present in the service area, which poses a confidentiality concern. In this context, the problem of maximizing the minimum secure energy efficiency (SEE) among all users is considered, subject to constraints on QoS, maximum transmit power, and maximum reflection power at the two metasurfaces. Specifically, the main contributions of this paper are:

- We consider a MISO system where a BS communicates with multiple mobile users through *two* metasurfaces. An RIS is deployed far from the transmitter and receivers to enhance the signal propagation, while an RHS is deployed in the near-field of the transmit antenna array of the BS. In addition, the BS employs the artificial noise technique to further enhance the secrecy of the commuication [37].
- In this context, we consider the problem of maximizing the minimum among the users' SEEs, with respect to the reflection coefficients of the RHS and RIS, as well as the beaforming vectors and artificial noise covariance matrix. The resulting problem is a non-differentiable, non-convex, fractional program, which can not be tackled by available methods. We develop a provably convergent approach that combines the generalized Dinkelbach's method, the sequential convex approximation (SCA) framework, the Schur complement method, and alternating optimization.
- Numerical results are provided to assess the advantages of the proposed method against alternative solutions based on digital antennas and/or only a RIS, thus analyzing the performance improvement provided by the use of the RHS at the BS.

2 System model and problem formulation

We consider a downlink multiple-input single-output (MISO) secure communication system, where a multi-antenna transmitter (Tx) with M antennas serves K legitimate single-antenna users in the presence of a single passive eavesdropper. The system model is depicted in Fig. 1.

To enhance the QoS and strengthen physical-layer security, the network is assisted by two metasurfaces, an RHS at the transmit side with N_t reflecting elements, and an RIS between the BS and the mobile users with N_r reflecting elements. Both the legitimate users and the eavesdropper receive the signals reflected by both the RHS and RIS. Let $\mathbf{Q}_t \in \mathbb{C}^{N_t \times M}$ be the channel from the Tx to the RHS, and $\mathbf{Q}_r \in \mathbb{C}^{N_r \times N_t}$ the channel from the RHS to the RIS. The channels from the RHS and RIS to user k are denoted

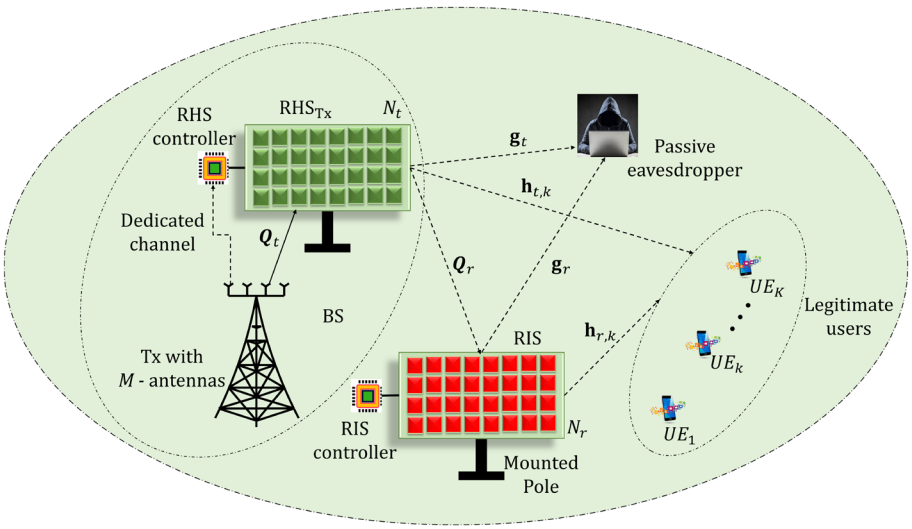

Fig. 1 Considered system model

by $\mathbf{h}_{t,k} \in \mathbb{C}^{N_t \times 1}$ and $\mathbf{h}_{r,k} \in \mathbb{C}^{N_r \times 1}$, respectively. Similarly, the channels to the eavesdropper from the RHS and RIS are $\mathbf{g}_t \in \mathbb{C}^{N_t \times 1}$ and $\mathbf{g}_r \in \mathbb{C}^{N_r \times 1}$. Define the RHS reflection coefficient matrix as $\mathbf{\Gamma}_t = \text{diag}(\beta_{t,1}, \ldots, \beta_{t,N})$ and the RIS reflection coefficient matrix as $\mathbf{\Gamma}_r = \text{diag}(\beta_{r,1}, \ldots, \beta_{r,N})$, respectively, where $\beta_{t,n}$ and $\beta_{r,n}$ are complex reflection coefficients. We consider nearly-passive metasurfaces with local reflection constraints, i.e. each reflecting element can not amplify the incoming signals, leading to the local constraints:

$$|\beta_{t,n}| = 1,\ n = 1, \ldots, N_t, \quad |\beta_{r,n}| = 1,\ n = 1, \ldots, N_r. \tag{1}$$

The effective channel to user k is $\mathbf{h}_k^{\text{eff}} = \left(\mathbf{h}_{t,k}^H \mathbf{\Gamma}_t \mathbf{Q}_t + \mathbf{h}_{r,k}^H \mathbf{\Gamma}_r \mathbf{Q}_r \mathbf{\Gamma}_t \mathbf{Q}_t\right)^H$, while the effective channel to the eavesdropper is $\mathbf{g}^{\text{eff}} = \left(\mathbf{g}_t^H \mathbf{\Gamma}_t \mathbf{Q}_t + \mathbf{g}_r^H \mathbf{\Gamma}_r \mathbf{Q}_r \mathbf{\Gamma}_t \mathbf{Q}_t\right)^H$. In order to enhance the secrecy of the legitimate communication, the transmitter employs the artificial noise (AN) technique, so that the transmitted signal is $\mathbf{x} = \sum_{k=1}^K \mathbf{w}_k s_k + \mathbf{z}$, where $\mathbf{w}_k \in \mathbb{C}^{M \times 1}$ is the beamforming vector intended for user k, s_k is the confidential message with $\mathbb{E}[|s_k|^2] = 1$, and $\mathbf{z}$ is artificial noise with covariance $\mathbf{C}_z = \mathbb{E}[\mathbf{z}\mathbf{z}^H]$. Given the above notation, the achievable rate of user k is:

$$R_k^{(u)} = \log_2\left(\frac{S_k^{(u)}}{I_k^{(u)}}\right), \tag{2}$$

where $S_k^{(u)} = \sum_{j=1}^K |\mathbf{h}_k^{\text{eff},H} \mathbf{w}_j|^2 + \mathbf{h}_k^{\text{eff},H} \mathbf{C}_z \mathbf{h}_k^{\text{eff}} + \sigma_{u,k}^2$ and $I_k^{(u)} = \sum_{j \neq k} |\mathbf{h}_k^{\text{eff},H} \mathbf{w}_j|^2 + \mathbf{h}_k^{\text{eff},H} \mathbf{C}_z \mathbf{h}_k^{\text{eff}} + \sigma_{u,k}^2$, and $n_{u,k} \sim \mathcal{CN}(0, \sigma_{u,k}^2)$ models the thermal noise at user k. Similarly, the eavesdropper's achievable rate corresponding to user k is

$$R_k^{(e)} = \log_2\left(\frac{S^{(e)}}{I_k^{(e)}}\right), \tag{3}$$

where $S^{(e)} = \sum_{j=1}^K |\mathbf{g}^{\text{eff},H} \mathbf{w}_j|^2 + \mathbf{g}^{\text{eff},H} \mathbf{C}_z \mathbf{g}^{\text{eff}} + \sigma_e^2$, $I_k^{(e)} = \sum_{j \neq k} |\mathbf{g}^{\text{eff},H} \mathbf{w}_j|^2 + \mathbf{g}^{\text{eff},H} \mathbf{C}_z \mathbf{g}^{\text{eff}} + \sigma_e^2$, and $n_e \sim \mathcal{CN}(0, \sigma_e^2)$ models the thermal noise at the eavesdropper. Thus, the secrecy rate associated to user k is.[1] $R_{\text{sec},k} = [R_k^{(u)} - R_k^{(e)}]^+$, and the corresponding secrecy energy efficiency (SEE) is

$$\eta_k = \frac{R_{\text{sec},k}}{P_{\text{total},k}}, \tag{4}$$

with $P_{\text{total},k}$ the total network power consumption, accounting for both the radiated power and the static power consumed in the system. The radiated power intended for user k can be expressed as $\|\mathbf{w}_k\|^2 + w_k \text{tr}(\mathbf{C}_z)$, with w_k a weight defining[2] what fraction of the artificial noise power is associated to user k. Instead, the total static power

[1] We assume that the system setup is such that it is possible to ensure a non-negative secrecy rate upon optimization, and hence, in the following, we neglect the non-negative operator $^+$

[2] We define weights $\{w_k\}$ using the softmax function:

$$w_k = \frac{\exp(\lambda R_{\min,k})}{\sum_{j=1}^K \exp(\lambda R_{\min,j})}, \tag{5}$$

where $\lambda > 0$ controls the sensitivity of the allocation.

consumption is $P_{\text{static}} = MP_{\text{Tx,static}} + N_t P_{\text{RHS,static}} + N_r P_{\text{RIS,static}} + P_{\text{other}}$, where $P_{\text{Tx,static}}$ is the per-antenna static power of the transmitter, $P_{\text{RHS,static}}$ and $P_{\text{RIS,static}}$ are the per-element static power consumptions of RHS and RIS, respectively, and P_{other} accounts for any additional fixed overhead sources. Hence, the total power consumption associated to user k is:

$$P_{\text{total},k} = \|\mathbf{w}_k\|^2 + w_k\left(P_{\text{static}} + \text{Tr}(\mathbf{C}_z)\right). \tag{6}$$

Substituting (6) into (4), we have:

$$\eta_k = \frac{R_{\text{sec},k}}{\|\mathbf{w}_k\|^2 + w_k\left(P_{\text{static}} + \text{Tr}(\mathbf{C}_z)\right)}. \tag{7}$$

In this context, the aim of this work is to maximize the minimum SEE over all users, subject to individual users' QoS constraints as well as metasurface reflection and power constraints. Namely, we consider the optimization problem

$$\max_{\{\mathbf{w}_k\},\mathbf{C}_z,\boldsymbol{\Gamma}_t,\boldsymbol{\Gamma}_r} \min_k \ \eta_k \tag{8a}$$

$$\text{s.t.} \quad R_k^{(u)} \geq R_{\min,k}, \quad \forall k, \tag{8b}$$

$$\sum_{k=1}^{K} \|\mathbf{w}_k\|^2 + \text{Tr}(\mathbf{C}_z) \leq P_{\max}, \tag{8c}$$

$$\left|\beta_{t,n}\right| = 1, \ n = 1, \ldots, N_t, \tag{8d}$$

$$|\beta_{r,n}| = 1, \ n = 1, \ldots, N_r. \tag{8e}$$

Problem (8) is a challenging fractional, non-convex problem, involving coupled optimization variables and constraints, which will be tackled by a combination of alternating maximization, generalized sequential fractional programming, and semidefinite programming.

3 Proposed solution method

Problem (8) is challenging for at least three reasons:

- The objective is a non-differentiable fractional function, which can not be tackled by standard fractional programming techniques, because the numerators of the K fractional functions in the objective, i.e. the users secrecy rates, are not concave in the optimization variables.
- The presence of two metasurfaces makes the optimization of the reflection coefficients more involved, because the two reflection matrices are not directly multiplied by each other, but are separated by the channel matrix $\boldsymbol{Q}_r$. This does not allow to reduce the metasurfaces design problem to the optimization of the product matrix $\boldsymbol{\Gamma}_r \boldsymbol{\Gamma}_t$.

- The QoS constraint is also non-convex, as the legitimate rate function is not concave in the optimization variables.

In the following, we will tackle Problem (8) by alternatively solving three subproblems, i.e. the optimization of the beamforming vectors and AN matrix $\{\mathbf{w}_k\}_{k=1}^K, \mathbf{C}_z\}$, of the RHS matrix $\mathbf{\Gamma}_T$, and of the RIS matrix $\mathbf{\Gamma}_R$.

3.1 Optimization of beamforming vectors and AN matrix

The problem to be solved is stated as

$$\max_{\{\mathbf{w}_k\},\mathbf{C}_z,\mathbf{\Gamma}_t,\mathbf{\Gamma}_r} \min_k \ \eta_k \tag{9a}$$

$$\text{s.t.} \quad R_k^{(u)} \geq R_{\min,k}, \quad \forall k, \tag{9b}$$

$$\sum_{k=1}^K \|\mathbf{w}_k\|^2 + \mathrm{Tr}(\mathbf{C}_z) \leq P_{\max}. \tag{9c}$$

The state-of-the-art method for the maximization of the minimum of a family of ratios is the generalized Dinkelbach's algorithm [38], which, for Problem (9), is stated as in Algorithm 1,

Algorithm 1 Genralized Dinkelbach's algorithm

$\varepsilon > 0$; $\lambda_{old} = 0$;
repeat
Let $\left(\{\mathbf{W}_k^\star\}_{k=1}^K, \mathbf{C}_z^\star\right)$ the solution of the following Problem (10)

$$\max_{\{\mathbf{W}_k\},\mathbf{C}_z} \min_k \ \left\{\{R_{sec,k}(\{\mathbf{w}_k\}_{k=1}^K, \mathbf{C}_z) - \lambda_{old}\left(\|\mathbf{w}_k\|^2 + w_k\big(P_{\text{static}} + \mathrm{Tr}(\mathbf{C}_z)\big)\right)\right\} \tag{10a}$$

$$\text{s.t.} \quad \widetilde{R}_u(\{\mathbf{w}_k\}_{k=1}^K, \mathbf{C}_z) \geq R_{\min,k}, \quad \forall k \tag{10b}$$

$$\sum_{k=1}^K \|\mathbf{w}_k\|^2 + \mathrm{Tr}(\mathbf{C}_z) \leq P_{\max} \tag{10c}$$

Compute

$$\lambda_{new} = \min_k \frac{R_{sec,k}(\{\mathbf{w}_k^\star\}_{k=1}^K, \mathbf{C}_z^\star)}{\|\mathbf{w}_k^\star\|^2 + w_k\big(P_{\text{static}} + \mathrm{Tr}(\mathbf{C}_z^\star)\big)} \tag{11}$$

$\mathrm{Err} = \lambda_{new} - \lambda_{old}$;
$\lambda_{old} = \lambda_{new}$;
until $\mathrm{Err} \leq \varepsilon$

which is guaranteed to converge to the global solution of Problem (9) and is typically faster than other available approaches, e.g. reformulating (9) in hypograph form and using the bisection method. Algorithm 1 iteratively updates the parameter λ_{old}, which is initialized to 0 and updated in each iteration according to (11), until the error $\lambda_{\text{new}} - \lambda_{\text{old}}$

is below the desired threshold ϵ. It can also be observed that the parameter λ_{new} that is updated in each iteration n, is the minimum SEE that is achieved in iteration n. Moreover, the generalized Dineklbach's method monotonically increases the value of the objective function of the global solution of Problem (10). For this reason, the error in each iteration can be evaluated as $\lambda_{\text{new}} - \lambda_{\text{old}}$, without any modulus operator. However, Problem (10) is extremely challenging to solve globally, due to its non-differentiable and non-convex form. Aiming at an algorithm with more practical complexity, the rest of this section is devoted to the development of a convex, yet suboptimal, reformulation of (10). This means that, in some iteration, it can happen that $\lambda_{\text{new}} - \lambda_{\text{old}}$ may become negative. In this case, the algorithm stops since $\text{Err} < 0 < \varepsilon$. In other words, Algorithm 1 monotonically increases the value of the minimum SEE for as many iterations as possible, and stops when either the global maximum of the minimum SEE is achieved, or the suboptimality of the solution of Problem (10) prevents from further increasing the minimum SEE function. In either case, Algorithm 1 monotonically increases the value of the minimum SEE in each iteration. A first challenge in tackling (10) lies in the fact that the objective function is not concave with respect to $(\{\mathbf{w}_k\}_{k=1}^K, \mathbf{C}_z)$. In order to address this issue, for all $k = 1, \ldots, K$, we define $\mathbf{W}_k = \mathbf{w}_k \mathbf{w}_k^H$, $\mathbf{H}_k^{\text{eff}} = \mathbf{h}_k^{\text{eff}} \left(\mathbf{h}_k^{\text{eff}}\right)^H \in \mathbb{C}^{M \times M}$ and $\mathbf{G}^{\text{eff}} = \mathbf{g}^{\text{eff}} \left(\mathbf{g}^{\text{eff}}\right)^H \in \mathbb{C}^{M \times M}$, which allows rewriting $R_k^{(u)}$ and $R_k^{(e)}$ as

$$R_k^{(u)} = \underbrace{\log_2\left(\sum_k \text{Tr}(\mathbf{H}_k^{\text{eff}}(\mathbf{W}_k + \mathbf{C}_z)) + \sigma_{u,k}^2\right)}_{g_{1,k}^{(u)}(\{\mathbf{W_k}\}_{k=1}^K, \mathbf{C}_z)} - \underbrace{\log_2\left(\sum_{j \neq k} \text{Tr}(\mathbf{H}_k^{\text{eff}}(\mathbf{W}_j + \mathbf{C}_z)) + \sigma_{u,k}^2\right)}_{g_{2,k}^{(u)}(\{\mathbf{W_j}\}_{j=1}^K, \mathbf{C}_z)} \tag{12}$$

$$R_k^{(e)} = \underbrace{\log_2\left(\sum_k \text{Tr}(\mathbf{G}^{\text{eff}}(\mathbf{W}_k + \mathbf{C}_z)) + \sigma_e^2\right)}_{g_1^{(e)}(\{\mathbf{W_k}\}_{k=1}^K, \mathbf{C}_z)} - \underbrace{\log_2\left(\sum_{j \neq k} \text{Tr}(\mathbf{G}^{\text{eff}}(\mathbf{W}_j + \mathbf{C}_z)) + \sigma_e^2\right)}_{g_{2,k}^{(e)}(\{\mathbf{W_k}\}_{k=1}^K, \mathbf{C}_z)}. \tag{13}$$

Then, the k-th user's secrecy rate can be expressed, with respect to $(\{\mathbf{W_k}\}_{k=1}^K, \mathbf{C}_z)$ as the difference of concave functions, i.e. $R_{sec,k} = g_{1,k}^{(u)} + g_{2,k}^{(e)} - \left(g_{2,k}^{(u)} + g_1^{(e)}\right)$. This allows resorting to the sequential programming framework, which can deal with the difference of concave functions by taking the first-order Taylor expansion of the convex term $-\left(g_{2,k}^{(u)} + g_1^{(e)}\right)$ around any given point $\mathbf{C}_z^{(n)}$ and $\mathbf{W}_k^{(n)}$, for all $k = 1, \ldots, K$. Then, we have:

$$\begin{aligned} -g_{2,k}^{(u)} = -\log_2\left(I_k^{(u)}\right) \geq & -\log_2\left(I_k^{(u)(n)}\right) \\ & - \frac{1}{I_k^{(u)(n)} \ln 2} \text{Tr}\left(\sum_{j \neq k} 2\Re\left\{\left(\nabla_{\mathbf{W}_j} I_k^{(u)(n)}\right)^H \left(\mathbf{W}_j - \mathbf{W}_j^{(n)}\right)\right\}\right. \\ & \left. + 2\Re\left\{\left(\nabla_{\mathbf{C}_z} I_k^{(u)(n)}\right)^H \left(\mathbf{C}_z - \mathbf{C}_z^{(n)}\right)\right\}\right) = \widetilde{g}_{2,k}^{(u)}. \end{aligned} \tag{14}$$

Similarly, for the convex term $-\log_2\left(S^{(e)}\right)$:

$$-g_1^{(e)} = -\log_2\left(S^{(e)}\right) \geq -\log_2\left(S^{(e)(n)}\right) - \frac{1}{S^{(e)(n)}\ln 2}\mathrm{Tr}\left(2\Re\left\{\left(\nabla_{\mathbf{W}_k} S^{(e)(n)}\right)^H\left(\mathbf{W}_k - \mathbf{W}_k^{(n)}\right)\right\} + 2\Re\left\{\left(\nabla_{\mathbf{C}_z} S^{(e)(n)}\right)^H\left(\mathbf{C}_z - \mathbf{C}_z^{(n)}\right)\right\}\right) = \widetilde{g}_1^{(e)}. \quad (15)$$

By applying these bounds we obtain $R_{sec,k}(\{\mathbf{W}_k\}_{k=1}^K, \mathbf{C}_z) \geq g_{1,k}^{(u)} + g_{2,k}^{(e)} + \widetilde{g}_{2,k}^{(u)} + \widetilde{g}_1^{(e)} = \widetilde{R}_{sec,k}(\{\mathbf{W}_k\}_{k=1}^K, \mathbf{C}_z)$. Moreover, it also holds that $g_{1,k}^{(u)} - g_{2,k}^{(u)} \geq g_{1,k}^{(u)} - \widetilde{g}_{2,k}^{(u)} = \widetilde{R}_k^{(u)}(\{\mathbf{W}_k\}_{k=1}^K, \mathbf{C}_z)$, with $\widetilde{R}_k^{(u)}(\{\mathbf{W}_k\}_{k=1}^K, \mathbf{C}_z)$ being a concave function. Then, a surrogate of Problem (10), which fulfills the assumptions of the sequential programming method can be stated as

$$\max_{\{\mathbf{W}_k \succeq \mathbf{0}\}, \mathbf{C}_z} \min_k \widetilde{R}_{sec,k}(\{\mathbf{W}_k\}_{k=1}^K, \mathbf{C}_z) - \lambda_{old}\left(\mathrm{Tr}(\mathbf{W}_k) + w_k\left(P_{\text{static}} + \mathrm{Tr}(\mathbf{C}_z)\right)\right) \quad (16a)$$

$$\text{s.t.} \quad \widetilde{R}_k^{(u)}\{\mathbf{W}_k \succeq \mathbf{0}\}_{k=1}^K, \mathbf{C}_z) \geq R_{\min,k}, \quad \forall k \quad (16b)$$

$$\sum_{k=1}^K \mathrm{Tr}(\mathbf{W}_k) + \mathrm{Tr}(\mathbf{C}_z) \leq P_{\max} \quad (16c)$$

$$\mathrm{rank}(\mathbf{W}_k) = 1\ ,\ \forall k = 1, \ldots, K\ , \quad (16d)$$

where we have introduced the rank-one constraints in (16d) since we set $\mathbf{W}_k = \mathbf{w}_k\mathbf{w}_k^H$. Problem (16d) has now a concave objective since the minimum of concave functions is concave, and also all constraints are in concave form, except for the newly added constraint in (16d). A popular way of tackling rank-one constraints is to employ the semidefinite relaxation method. However, in the case of Problem (16d), this approach does not offer any guarantee as to the rank of the solution of the relaxed problem. Thus, semidefinite relaxation may require to employ rank reduction techniques to come up with a feasible solution, which may cause significant performance degradation. Instead, here we employ a different method, which is based on a penalty approach. To elaborate, for any $k = 1, \ldots, K$, let us assume, without loss of generality, that the eigenvalues, $\mu_1, \ldots, \mu_M$, of $\mathbf{W}_k$ are ordered in increasing order of magnitude. Then, the quantity

$$\mathrm{Tr}(\mathbf{W}_k) - \mu_1(\mathbf{W}_k) = \sum_{i=2}^M \mu_i(\mathbf{W}_k)\ , \quad (17)$$

is a measure of how far from a rank-one matrix $\mathbf{W}_k$ is. Indeed, the quantity in (17) is non-negative, since $\mathbf{W}_k \succeq \mathbf{0}$, and it is zero if and only if $\mathrm{rank}(\mathbf{W}_k) = 1$. Then, we reformulate Problem (16a) by adopting a barrier method including (17) in the objective as a penalty term, which yields

$$\max_{\{\mathbf{W}_k \succeq \mathbf{0}\},\mathbf{C}_z} \min_k \left\{ \{\widetilde{R}_{sec,k}(\{\mathbf{W}_k\}_{k=1}^K, \mathbf{C}_z) - \lambda_{old}\left(\mathrm{Tr}(\mathbf{W}_k) + w_k\left(P_{\mathrm{static}} + \mathrm{Tr}(\mathbf{C}_z)\right)\right)\right\} + \sum_{k=1}^K \alpha_k(-\mathrm{Tr}(\mathbf{W}_k) + \mu_1(\mathbf{W}_k)) \tag{18a}$$

$$\text{s.t.} \quad \widetilde{R}_u(\{\mathbf{W}_k\}_{k=1}^K, \mathbf{C}_z) \geq R_{\min,k}, \quad \forall k \tag{18b}$$

$$\sum_{k=1}^K \mathrm{Tr}(\mathbf{W}_k) + \mathrm{Tr}(\mathbf{C}_z) \leq P_{\max}, \tag{18c}$$

wherein $\alpha_k > 0$ is a barrier penalty coefficient that can be chosen in order to make the barrier stricter or milder. The last difficulty lies in the fact that $\mu_1(\mathbf{W}_k)$ is a convex function, being a norm. Then, we lower-bound it by computing its first-order Taylor expansion around the point $\mathbf{W}_k^{(n)}$, which yields the following linear lower-bound

$$\mu_1(\mathbf{W}_k) \geq \mu_1(\mathbf{W}_k^{(n)}) + 2\Re\left\{\mathrm{Tr}\left(\nabla_{\mathbf{W}_k}\mu_1(\mathbf{W}_k^{(n)})^H\left(\mathbf{W}_k - \mathbf{W}_k^{(n)}\right)\right)\right\} = \widetilde{G}_k(\mathbf{W}_k), \tag{19}$$

with $\nabla_{\mathbf{W}_k}\mu_1(\mathbf{W}_k^{(n)}) = \mathbf{u}_1^{(n)}\mathbf{u}_1^{(n)H}$, where $\mathbf{u}_1^{(n)}$ is the eigenvector corresponding to the maximum eigenvalue μ_1. Then, Problem (18) can be further reformulated as

$$\max_{\{\mathbf{W}_k \succeq \mathbf{0}\},\mathbf{C}_z} \min_k \left\{ \{\widetilde{R}_{sec,k}(\{\mathbf{W}_k\}_{k=1}^K, \mathbf{C}_z) - \lambda_{old}\left(\mathrm{Tr}(\mathbf{W}_k) + w_k\left(P_{\mathrm{static}} + \mathrm{Tr}(\mathbf{C}_z)\right)\right)\right\} + \sum_{k=1}^K \alpha_k\left(-\mathrm{Tr}(\mathbf{W}_k) + \widetilde{G}_k(\mathbf{W}_k)\right) \tag{20a}$$

$$\text{s.t.} \quad \widetilde{R}_u(\{\mathbf{W}_k\}_{k=1}^K, \mathbf{C}_z) \geq R_{\min,k}, \quad \forall k \tag{20b}$$

$$\sum_{k=1}^K \mathrm{Tr}(\mathbf{W}_k) + \mathrm{Tr}(\mathbf{C}_z) \leq P_{\max}, \tag{20c}$$

and a sequential fractional programming (SFP) algorithm to tackle Problem (10) can be stated as in Algorithm 2, with F denoting (20a).

Algorithm 2 SFP for Problem (10)

$\varepsilon > 0$; `Set feasible values for` $\mathbf{C}_z^{(n)}$, $\mathbf{W}_k^{(n)}$ for all $k = 1, \ldots, K$;
repeat
  `Let` $\left(\{\mathbf{W}_k^\star\}_{k=1}^K, \mathbf{C}_z^\star\right)$ `be the solution of Problem` (20);
  $\mathrm{Err} = \left| F\left(\{\mathbf{W}_k^{(n)}\}_{k=1}^K, \mathbf{C}_z^n\right) - F\left(\{\mathbf{W}_k^\star\}_{k=1}^K, \mathbf{C}_z^\star\right)\right|$;
  $\mathbf{C}_z^{(n)} = \mathbf{C}_z^\star$, $\mathbf{W}_k^{(n)} = \mathbf{W}_k^\star$ for all $k = 1, \ldots, K$;
until $\mathrm{Err} \leq \varepsilon$

3.2 Optimization of $\mathbf{\Gamma}_T$

With respect to $\mathbf{\Gamma}_T$, for fixed $\mathbf{\Gamma}_R$, $\{\mathbf{w}_k\}_{k=1}^K$, $\mathbf{C}_z$, Problem (8) becomes

$$\max_{\mathbf{\Gamma}_t} \min_k R_{sec,k} \tag{21a}$$

$$\text{s.t.} \quad R_k^{(u)} \geq R_{\min,k}, \quad \forall k, \tag{21b}$$

$$\left|\beta_{t,n}\right| = 1, \ n = 1, \ldots, N_t. \tag{21c}$$

and we notice that the objective reduces to the secrecy rate, since the denominator of the SEE does not depend on the metasurface matrices. Nevertheless, the problem is still not convex, since neither the users' secrecy rates nor the legitimate rates are concave functions of $\mathbf{\Gamma}_t$. To address these issues, we apply again the sequential programming framework. To this end, let us define the matrices $\mathbf{X}_t = \boldsymbol{\gamma}_t^* \boldsymbol{\gamma}_t^T$, $\mathbf{B}_e = \mathbf{Q}_t^H \text{diag}(\mathbf{g}_t + \mathbf{Q}_r^H \mathbf{\Gamma}_r^H \mathbf{g}_r)$ $\mathbf{B}_k = \mathbf{Q}_t^H \text{diag}(\mathbf{h}_{t,k} + \mathbf{Q}_r^H \mathbf{\Gamma}_r^H \mathbf{h}_{r,k})$, for all $k = 1, \ldots, K$. Then, it holds that

$$\begin{aligned} R_k^{(u)} = & \underbrace{\log_2 \left(\sum_{j=1}^{K} \text{Tr}(\mathbf{B}_k \mathbf{X}_t \mathbf{B}_k^H \mathbf{W}_j) + \text{Tr}(\mathbf{B}_k \mathbf{X}_t \mathbf{B}_k^H \mathbf{C}_z) + \sigma_{u,k}^2 \right)}_{f_{1,k}^{(u)}(\mathbf{X}_t)} \\ & \underbrace{- \log_2 \left(\sum_{j \neq k} \text{Tr}(\mathbf{B}_k \mathbf{X}_t \mathbf{B}_k^H \mathbf{W}_j) + \text{Tr}(\mathbf{B}_k \mathbf{X}_t \mathbf{B}_k^H \mathbf{C}_z) + \sigma_{u,k}^2 \right)}_{f_{2,k}^{(u)}(\mathbf{X}_t)} \end{aligned} \tag{22}$$

$$\begin{aligned} R_k^{(e)} = & \underbrace{\log_2 \left(\sum_{j=1}^{K} \text{Tr}(\mathbf{B}_e \mathbf{X}_t \mathbf{B}_e^H \mathbf{W}_j) + \text{Tr}(\mathbf{B}_e \mathbf{X}_t \mathbf{B}_e^H \mathbf{C}_z) + \sigma_e^2 \right)}_{f_1^{(e)}(\mathbf{X}_t)} \\ & \underbrace{- \log_2 \left(\sum_{j \neq k} \text{Tr}(\mathbf{B}_e \mathbf{X}_t \mathbf{B}_e^H \mathbf{W}_j) + \text{Tr}(\mathbf{B}_e \mathbf{X}_t \mathbf{B}_e^H \mathbf{C}_z) + \sigma_e^2 \right)}_{f_{2,k}^{(e)}(\mathbf{X}_t)} \end{aligned} \tag{23}$$

Then, $R_{sec,k} = R_k^{(u)} - R_k^{(e)} = f_{1,k}^{(u)} + f_{2,k}^{(e)} - (f_{2,k}^{(u)} + f_1^{(e)})$, and it can be seen that both $f_{1,k}^{(u)} + f_{2,k}^{(e)}$ and $f_{2,k}^{(u)} + f_1^{(e)}$ are concave functions in $\mathbf{X}_t$. Thus, a concave lower-bound of $R_{\text{sec},k}$ can be obtained by computing the first-order Taylor expansion of $(f_{2,k}^{(u)} + f_1^{(e)})$ around any feasible point $\mathbf{X}_t^{(n)}$. Namely, it holds

$$-f_{2,k}^{(u)} = -\log_2\left(I_k^{(u)}\right) \geq -\log_2\left(I_k^{(u)(n)}\right) - \frac{1}{\ln 2} \frac{1}{I_k^{(u)(n)}} 2\Re\left\{\text{Tr}\left(\left(\nabla_{I_k}^{(u)(n)}\right)^H (\mathbf{X}_t - \mathbf{X}_t^{(n)})\right)\right\} = \widetilde{f}_{2,k}^{(u)} \tag{24}$$

$$-f_1^{(e)} = -\log_2\left(S^{(e)}\right) \geq -\log_2\left(S^{(e)(n)}\right) - \frac{1}{\ln 2}\frac{1}{S^{(e)(n)}} 2\Re\left\{\mathrm{Tr}\left(\left(\nabla_S^{(e)(n)}\right)^H (\mathbf{X}_t - \mathbf{X}_t^{(n)})\right)\right\} = \widetilde{f}_1^{(e)} \tag{25}$$

wherein $I_k^{(u)(n)}$ and $S^{(e)(n)}$ are $I_k^{(u)}$ and $S^{(e)}$ evaluated at $\mathbf{X}_t^{(n)}$, respectively, and the gradients are:

$$\nabla_{I_k}^{(u)(n)} = \sum_{j \neq k} \mathbf{B}_k^H \mathbf{W}_j \mathbf{B}_k + \mathbf{B}_k^H \mathbf{C}_z \mathbf{B}_k, \tag{26}$$

$$\nabla_S^{(e)(n)} = \sum_{j=1}^{K} \mathbf{B}_e^H \mathbf{W}_j \mathbf{B}_e + \mathbf{B}_e^H \mathbf{C}_z \mathbf{B}_e. \tag{27}$$

Then, we have that $R_{sec,k} \geq f_{1,k}^{(u)} + f_{2,k}^{(e)} + \widetilde{f}_{2,k}^{(u)} + \widetilde{f}_1^{(e)} = \widetilde{R}_{sec,k}$ and $R_k^{(u)} \geq f_{1,k}^{(u)} + \widetilde{f}_{2,k}^{(u)} = \widetilde{R}_k^{(u)}$, which yields the following surrogate of Problem (21)

$$\max_{\boldsymbol{X}_t} \min_k \widetilde{R}_{sec,k} \tag{28a}$$

$$\text{s.t.} \quad \widetilde{R}_k^{(u)} \geq R_{\min,k}, \quad k = 1, \ldots, K \tag{28b}$$

$$\mathbf{X}_t(n,n) = 1, \ n = 1, \ldots, N_t \tag{28c}$$

$$\mathrm{rank}(\mathbf{X}_t) = 1. \tag{28d}$$

Finally, it remains to deal with the constraint in (28d). Following a similar method as in Section 3.1, the quantity $\mathrm{Tr}(\mathbf{X}_t) - \mu_1(\mathbf{X}_t)$, with $\mu_1(\mathbf{X}_t)$ the maximum eigenvalue of $\mathbf{X}_t$, is embedded as a barrier in the objective to promote low-rank solutions. A lower-bound of $\mu_1(\mathbf{X}_t)$ is obtained by the first-order Taylor expansion around $\mathbf{X}_t^{(n)}$,

$$\mu_1(\mathbf{X}_t) \geq \mu_1(\mathbf{X}_t^{(n)}) + 2\Re\left\{\mathrm{Tr}\left(\nabla_{\mathbf{X}_t}\mu_1(\mathbf{X}_t^{(n)})^H \left(\mathbf{X}_t - \mathbf{X}_t^{(n)}\right)\right)\right\} = F_t(\mathbf{X}_t), \tag{29}$$

with $\nabla_{\mathbf{X}_t}\mu_1(\mathbf{X}_t^{(n)}) = \mathbf{v}_{1,t}^{(n)}\mathbf{v}_{1,t}^{(n)H}$, where $\mathbf{v}_1^{(n)}$ is the eigenvector corresponding to the eigenvalue μ_1. Then, in each iteration of the sequential algorithm we should solve:

$$\max_{\boldsymbol{X}_t} \min_k \widetilde{R}_{sec,k} + \alpha(-\mathrm{Tr}(\mathbf{X}_t) + F_t(\mathbf{X}_t)) \tag{30a}$$

$$\text{s.t.} \quad \widetilde{R}_k^{(u)} \geq R_{\min,k}, \quad \forall k, \tag{30b}$$

$$\mathbf{X}_t(n,n) = 1, \ n = 1, \ldots, N_t \ , \tag{30c}$$

which can be seen to be convex. Thus, the sequential optimization algorithm is formulated as in Algorithm 3, with $T(\cdot)$ denoting the objective in (30a).

Algorithm 3 SFP for (21)

$\varepsilon > 0$; Set feasible values for $\mathbf{X}_t^{(n)}$;
repeat
  Let $\mathbf{X}_t^{\star}$ be the solution of Problem (30);
  $\text{Err} = \left| T(\mathbf{X}_t^{(n)}) - T(\mathbf{X}_t^{\star}) \right|$;
  $\mathbf{X}_t^{(n)} = \mathbf{X}_t^{\star}$;
until $\text{Err} \leq \varepsilon$

3.3 Optimization of $\mathbf{\Gamma}_R$

With respect to $\mathbf{\Gamma}_R$, for fixed $\mathbf{\Gamma}_T$, $\{\mathbf{w}_k\}_{k=1}^K$, $\mathbf{C}_z$, Problem (8) becomes

$$\max_{\mathbf{\Gamma}_t} \min_k R_{sec,k} \tag{31a}$$

$$\text{s.t.} \quad R_k^{(u)} \geq R_{\min,k}, \quad \forall k, \tag{31b}$$

$$|\beta_{r,n}| = 1, \ n = 1, \ldots, N_r. \tag{31c}$$

To elaborate, we first define the augmented $(N_r + 1) \times 1$ vector $\widehat{\boldsymbol{\gamma}}_r = [\boldsymbol{\gamma}_r^T 1]^T$. Then, we define $\mathbf{X}_r = \boldsymbol{\gamma}_r^* \boldsymbol{\gamma}_r^T$, $\widehat{\mathbf{X}}_r = \widehat{\boldsymbol{\gamma}}_r^* \widehat{\boldsymbol{\gamma}}_r^T$, and

$$\mathbf{C}_k = \left[\mathbf{Q}_t^H \mathbf{\Gamma}_t^H \mathbf{Q}_r^H \text{diag}(\mathbf{h}_{r,k}) \ \mathbf{Q}_t^H \mathbf{\Gamma}_t^H \mathbf{h}_{t,k} \right], \forall k = 1, \ldots, K \ . \tag{32}$$

$$\mathbf{C}_e = \left[\mathbf{Q}_t^H \mathbf{\Gamma}_t^H \mathbf{Q}_r^H \text{diag}(\mathbf{g}_r) \ \mathbf{Q}_t^H \mathbf{\Gamma}_t^H \mathbf{g}_t \right] \tag{33}$$

Then, it holds that

$$\begin{aligned} R_k^{(u)} = & \underbrace{\log_2 \left(\sum_{j=1}^{K} \text{Tr}(\mathbf{C}_k \widehat{\mathbf{X}}_r \mathbf{C}_k^H \mathbf{W}_j) + \text{Tr}(\mathbf{C}_k \widehat{\mathbf{X}}_r \mathbf{C}_k^H \mathbf{C}_z) + \sigma_{u,k}^2 \right)}_{f_{1,k}^{(u)}(\widehat{\mathbf{X}}_r)} \\ & - \underbrace{\log_2 \left(\sum_{j \neq k} \text{Tr}(\mathbf{C}_k \widehat{\mathbf{X}}_r \mathbf{C}_k^H \mathbf{W}_j) + \text{Tr}(\mathbf{C}_k \widehat{\mathbf{X}}_r \mathbf{C}_k^H \mathbf{C}_z) + \sigma_{u,k}^2 \right)}_{f_{2,k}^{(u)}(\widehat{\mathbf{X}}_r)} \end{aligned} \tag{34}$$

$$R_k^{(e)} = \underbrace{\log_2\left(\sum_{j=1}^{K} \mathrm{Tr}(\mathbf{C}_e\widehat{\mathbf{X}}_r\mathbf{C}_e^H\mathbf{W}_j) + \mathrm{Tr}(\mathbf{C}_e\widehat{\mathbf{X}}_r\mathbf{C}_e^H\mathbf{C}_z) + \sigma_e^2\right)}_{f_1^{(e)}(\widehat{\mathbf{X}}_r)} - \underbrace{\log_2\left(\sum_{j\neq k} \mathrm{Tr}(\mathbf{C}_e\widehat{\mathbf{X}}_r\mathbf{C}_e^H\mathbf{W}_j) + \mathrm{Tr}(\mathbf{C}_e\widehat{\mathbf{X}}_r\mathbf{C}_e^H\mathbf{C}_z) + \sigma_e^2\right)}_{f_{2,k}^{(e)}(\widehat{\mathbf{X}}_r)} \tag{35}$$

Then, $R_{sec,k} = R_k^{(u)} - R_k^{(e)} = f_{1,k}^{(u)} + f_{2,k}^{(e)} - (f_{2,k}^{(u)} + f_1^{(e)})$, and it can be seen that both $f_{1,k}^{(u)} + f_{2,k}^{(e)}$ and $f_{2,k}^{(u)} + f_1^{(e)}$ are concave functions in $\widehat{\mathbf{X}}_r$. Thus, a concave lower-bound of $R_{\mathrm{sec},k}$ can be obtained by computing the first-order Taylor expansion of $(f_{2,k}^{(u)} + f_1^{(e)})$ around any feasible point $\widehat{\mathbf{X}}_r^{(n)}$. Namely, it holds

$$-f_{2,k}^{(u)} = -\log_2\left(I_k^{(u)}\right) \geq -\log_2\left(I_k^{(u)(n)}\right) - \frac{1}{\ln 2}\frac{1}{I_k^{(u)(n)}} 2\Re\left\{\mathrm{Tr}\left(\left(\nabla_{I_k}^{(u)(n)}\right)^H(\widehat{\mathbf{X}}_r - \widehat{\mathbf{X}}_r^{(n)})\right)\right\} = \widetilde{f}_{2,k}^{(u)} \tag{36}$$

$$-f_1^{(e)} = -\log_2\left(S^{(e)}\right) \geq -\log_2\left(S^{(e)(n)}\right) - \frac{1}{\ln 2}\frac{1}{S^{(e)(n)}} 2\Re\left\{\mathrm{Tr}\left(\left(\nabla_S^{(e)(n)}\right)^H(\widehat{\mathbf{X}}_r - \widehat{\mathbf{X}}_r^{(n)})\right)\right\} = \widetilde{f}_1^{(e)} \tag{37}$$

wherein $I_u^{(k)(n)}$ and $S^{(e)(n)}$ are $I_k^{(u)}$ and $S^{(e)}$ evaluated at $\widehat{\mathbf{X}}_r^{(n)}$, respectively, and the gradients can be computed by similar formulas as in (26) and (27). Then, we have that $R_{\mathrm{sec},k} \geq f_{1,k}^{(u)} + f_{2,k}^{(e)} + \widetilde{f}_{2,k}^{(u)} + \widetilde{f}_1^{(e)} = \widetilde{R}_{\mathrm{sec},k}$ and $R_k^{(u)} \geq f_{1,k}^{(u)} + \widetilde{f}_{2,k}^{(u)} = \widetilde{R}_k^{(u)}$, which yields the following surrogate of Problem (31)

$$\max_{\boldsymbol{X}_r \succeq \mathbf{0}} \min_k \widetilde{R}_{\mathrm{sec},k} \tag{38a}$$

$$\text{s.t.} \quad \widetilde{R}_k^{(u)} \geq R_{\min,k}, \quad \forall k, \tag{38b}$$

$$\widehat{\mathbf{X}}_r(n,n) = 1, \ n = 1,\ldots,N_r+1 \tag{38c}$$

$$\mathrm{rank}(\widehat{\mathbf{X}}_r) = 1\,, \tag{38d}$$

where the constraint in (38d) ensures that any solution of Problem (38) can be written as an outer product of the form $\widehat{\boldsymbol{\gamma}_r^*}\widehat{\boldsymbol{\gamma}_r^T}$. Moreover, it should be observed that there is a phase ambiguity in the choice of $\widehat{\boldsymbol{\gamma}}_r$, i.e. $\widehat{\boldsymbol{\gamma}}_r$ and $e^{i\theta}\widehat{\boldsymbol{\gamma}}_r$ yield the same matrix $\widehat{\boldsymbol{X}}_r$ and also the same matrix $\boldsymbol{X}_r$. However, in order to ensure consistency with the definition of $\widehat{\boldsymbol{\gamma}}_r$, the phase θ should be chosen so as to have $\widehat{\boldsymbol{\gamma}}_r(N_r+1) = 1$.

Finally, the rank-one constraint in (38d) can be dealt with as in Section 3.2, which leads to the following convex reformulation of Problem (38):

$$\max_{\boldsymbol{X}_r} \min_k \widetilde{R}_{sec,k} + \alpha(-\mathrm{Tr}(\mathbf{X}_r) + F_r(\mathbf{X}_r)) \tag{39a}$$

$$\text{s.t.} \quad \widetilde{R}_k^{(u)} \geq R_{\min,k}, \quad \forall k, \tag{39b}$$

$$\mathbf{X}_r(n,n) = 1, \; n = 1, \ldots, N_r + 1 \,, \tag{39c}$$

wherein

$$F_r(\mathbf{X}_r) = \mu_1(\mathbf{X}_r^{(n)}) + 2\Re\left\{\mathrm{Tr}\left(\nabla_{\mathbf{X}_r}\mu_1(\mathbf{X}_r^{(n)})^H\left(\mathbf{X}_r - \mathbf{X}_r^{(n)}\right)\right)\right\} \tag{40}$$

with $\nabla_{\mathbf{X}_r}\mu_1(\mathbf{X}_r^{(n)}) = \mathbf{v}_{1,r}^{(n)}\mathbf{v}_{1,r}^{(n)H}$, where $\mathbf{v}_{1,r}^{(n)}$ is the eigenvector corresponding to μ_1, which is the maximum eigenvalue of $\mathbf{X}_r$.

Thus, the sequential optimization algorithm is formulated as in Algorithm 4, with $R(\cdot)$ denoting the objective in (31a).

Algorithm 4 SFP for problem (31)

$\varepsilon > 0$; `Set feasible values for` $\mathbf{X}_r^{(n)}$;
repeat
  `Let` $\mathbf{X}_r^\star$ `be the solution of Problem` (39a);
  $\mathrm{Err} = \left|R(\mathbf{X}_r^{(n)}) - R(\mathbf{X}_r^\star)\right|$;
  $\mathbf{X}_r^{(n)} = \mathbf{X}_r^\star$;
until $\mathrm{Err} \leq \varepsilon$

3.4 Overall algorithm and computational complexity

Based on previous derivations, an alternating optimization algorithm for Problem (8) can be stated as in Algorithm 5, with O denoting the objective of Problem (8). It should be noted that, while Algorithm 5 has been developed for the maximization of the minimum SEE, it can be specialized to maximize the secrecy rate. Indeed, the minimum secrecy rate is obtained from the minimum SEE by removing the denominator in (7), for all $k = 1, \ldots, K$. Then, all the optimization algorithms developed for the minimum of the users' SEE can operate also only on the numerators of the users' SEE, to perform minimum secrecy rate maximization.

Algorithm 5 Alternating optimization for problem (8)

$\varepsilon > 0$; $n = 0$; `Set feasible values for` $\{\boldsymbol{w}_{k,n}\}_{k=1}^K$, $\boldsymbol{C}_{z,n}$, $\boldsymbol{\Gamma}_{t,n}$, $\boldsymbol{\Gamma}_{r,n}$;
repeat
  $n = n + 1$;
  `Let` $\{\boldsymbol{w}_{k,n}\}_{k=1}^K$, $\boldsymbol{C}_z$ `be the output of Algorithm` 1 `given` $\boldsymbol{\Gamma}_{t,n-1}$, $\boldsymbol{\Gamma}_{r,n-1}$;
  `Let` $\boldsymbol{\Gamma}_{t,n}$ `be the output of Algorithm` 3 `given` $\{\boldsymbol{w}_{k,n}\}_{k=1}^K$, $\boldsymbol{C}_{z,n}$, $\boldsymbol{\Gamma}_{r,n-1}$;
  `Let` $\boldsymbol{\Gamma}_{r,n}$ `be the output of Algorithm` 4 `given` $\{\boldsymbol{w}_{k,n}\}_{k=1}^K$, $\boldsymbol{C}_{z,n}$, $\boldsymbol{\Gamma}_{t,n}$;
  $\mathrm{Err} = \left|O\left(\{\boldsymbol{w}_{k,n}\}_{k=1}^K, \boldsymbol{C}_{z,n}, \boldsymbol{\Gamma}_{t,n}, \boldsymbol{\Gamma}_{r,n}\right) - O\left(\{\boldsymbol{w}_{k,n-1}\}_{k=1}^K, \boldsymbol{C}_{z,n-1}, \boldsymbol{\Gamma}_{t,n-1}, \boldsymbol{\Gamma}_{r,n-1}\right)\right|$;
until $\mathrm{Err} \leq \varepsilon$

3.4.1 Convergence and optimality

Algorithm 5 is guaranteed to converge in the value of the objective of Problem (8), since, by construction, in each iteration, the value of the objective is not decreased. Indeed, as discussed in previous section, the generalized Dinkelbach's method in Algorithm 1, and the sequential methods in Algorithms 3 and 4 monotonically increase the value of the minimum SEE function. Thus, since the minimum SEE function does not diverge, Algorithm 5 must converge in the objective value. However, it can not be claimed that, upon convergence, the global maximum of the SEE function is achieved. This is due to the fact that all three subproblems in Algorithms 5 are not solved in a provably optimal way. Thus, convergence to a local optimum or other fixed points can happen. Nevertheless, as discussed previously, the goal of this work is not to determine the global solution of Problem (8), which would not be practical as it would entail an exponential complexity in the number of optimization variables, but rather to provide a more practical algorithm, which enjoys a polynomial complexity in the number of optimization variables, as discussed in the rest of this section.

3.4.2 Computational complexity

The asymptotic computational complexity of Algorithm 5 can be evaluated as

$$\mathcal{C}_{\text{alt}} = \mathcal{O}(I_{\text{alt}}(\mathcal{C}_{\text{Dink}} + \mathcal{C}_T + \mathcal{C}_R)) \,, \tag{41}$$

wherein I_{alt} is the number of iterations for Algorithm 5 to converge, while $\mathcal{C}_{\text{Dink}}$, $\mathcal{C}_T$, $\mathcal{C}_R$ are the asymptotic complexity of Algorithms 1, 3, and 4, respectively. All Algorithms 1, 3, and 4 involve the solution of a sequence of convex problems, and, thus, their complexity is polynomial in number of variables of each convex problems and scales linearly with the number of iterations to reach convergence. Thus, recalling that the complexity of a convex problem can be bounded by the fourth power of the number of variables [39], it follows that

$$\mathcal{C}_{\text{Dink}} = \mathcal{O}(I_{\text{Dink}} I_{\text{seq}}((M(M+1))^4)) \tag{42}$$

$$\mathcal{C}_T \leq \mathcal{O}\left(I_T \left(\frac{N_T(N_T-1)}{2}\right)^4\right) \tag{43}$$

$$\mathcal{C}_R \leq \mathcal{O}\left(I_R \left(\frac{N_R(N_R+1)}{2}\right)^4\right) . \tag{44}$$

wherein $\mathcal{C}_{\text{Dink}}$ holds upon denoting by I_{Dink} and I_{seq} the number of iterations for Algorithms 1 and 2 to converge, and observing that in each iteration of Algorithm 2 the convex problem (20) is solved, which optimizes two $M \times M$ Hermitian matrices and thus has $2\frac{M(M+1)}{2} = M(M+1)$ optimization variables; $\mathcal{C}_T$ holds upon denoting by I_T the number of iterations for Algorithm 3 to converge, and observing that, in each iteration of Algorithm 3, the convex Problem (30) is solved, which optimizes an Hermitian $N_T \times N_T$ matrix whose diagonal is constrained to have elements equal to 1. Thus, Problem (30) has $\frac{N_T(N_T-1)}{2}$ variables; similarly, $\mathcal{C}_R$ holds upon denoting by I_R the number of iterations

for Algorithm 4 to converge, and observing that, in each iteration of Algorithm 4, the convex Problem (39) is solved, which optimizes an Hermitian $N_R + 1 \times N_R + 1$ matrix whose diagonal is constrained to have elements equal to 1. Thus, Problem (39) has $\frac{N_R(N_R+1)}{2}$ variables.

4 Numerical results

For our numerical analysis, we have considered a BS that communicates with $K = 4$ single-antenna mobile users randomly placed in a cell with radius 50 m around the BS. The BS is placed at a height of 11 m from the ground, while the user equipments are placed at a height of 1.5 m. The carrier frequency is 3.5 GHz, the communication bandwidth is 20 MHz, the thermal noise power spectral density is -174 dBm/Hz, the noise figure at the receiver is 5 dB. The RIS is placed at an elevation of 10 m and both the RHS and RIS are equipped with 64 reflecting elements. Each element of the RHS and RIS consumes a static power of $P_{\text{RHS,static}} = P_{\text{RIS,static}} = 0$ dBm, each digital antenna of the BS, with the associated RF hardware chain, consumes a static power of $P_{\text{Tx,static}} = 24$ dBm, while the rest of the power consumption in the system is $P_{\text{other}} = 33$ dBm. The RIS is placed at a distance of 50 m from the BS, while the RHS is co-located with the BS antenna array. The channel from the BS to the RHS follows the deterministic spherical wave model [40, 41]. All other channels are subject to path-loss with power decay factor of 2 and Rice fading with Rice factor 5, except the channel from the RHS to the RIS, which has a Rice factor of 10. The choice of a higher Rice factor for the RHS-RIS channel is motivated by the consideration that these are fixed devices, which are placed in favorable positions to have a strong line-of-sight.

Figure 2 reports the achieved minimum SEE versus the maximum transmit power $P_{\max}$, assuming $R_{\min,k} = 0$ bit/s/Hz for all k, i.e. no QoS constraints are enforced, for the following resource allocation policies:

(a) Algorithm 5 for the maximization of the minimum SEE through the optimization of the RHS and RIS reflection matrices $\boldsymbol{\Gamma}_T$ and $\boldsymbol{\Gamma}_R$, and of the transmit beamforming vectors $\{\boldsymbol{w}_k\}_{k=1}^K$ and artificial noise covariance matrix $\boldsymbol{C}_z$. In this case, the base station is assumed to have an array with $M = 4$ digital antennas, while the RHS and RIS are equipped with $N_T = N_R = 64$ reflecting elements.

(b) Algorithm 5 for the maximization of the minimum of the secrecy rate through the optimization of the RHS and RIS reflection matrices $\boldsymbol{\Gamma}_T$ and $\boldsymbol{\Gamma}_R$, and of the transmit beamforming $\{\boldsymbol{w}_k\}_{k=1}^K$ and artificial noise covariance matrix $\boldsymbol{C}_z$. In this case, the base station is assumed to have an array with $M = 4$ digital antennas, while the RHS and RIS are equipped with $N_T = N_R = 64$ reflecting elements.

(c) Maximization of the minimum SEE through the optimization of the RIS reflection matrix $\boldsymbol{\Gamma}_R$, the transmit beamforming $\{\boldsymbol{w}_k\}_{k=1}^K$, and artificial noise covariance matrix $\boldsymbol{C}_z$. In this case, no RHS is considered, and the BS is assumed to have an array with $M = 32$ digital antennas, while the RIS is equipped with $N_R = 64$ reflecting elements. The maximization has been performed by Algorithm 5, by skipping the subroutine for the optimization of $\boldsymbol{\Gamma}_t$.

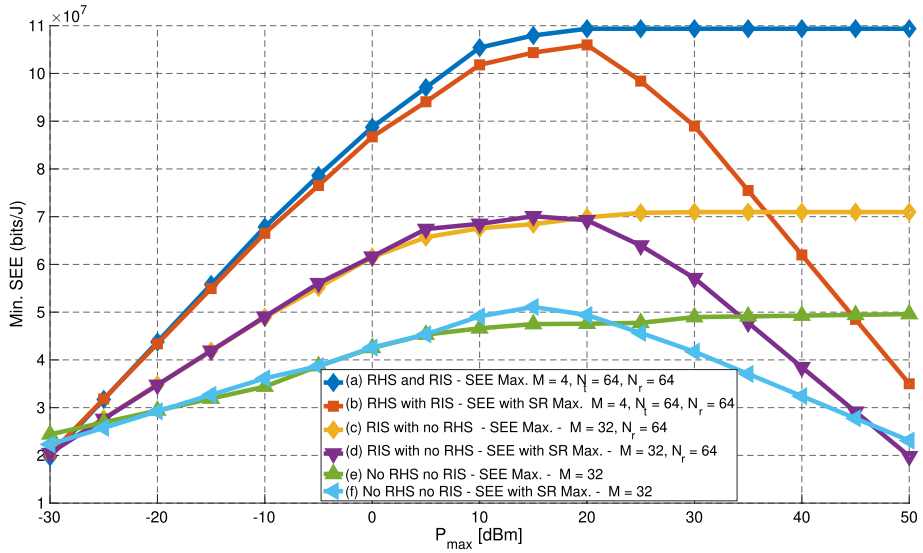

Fig. 2 Minimum SEE versus maximum transmit power for different resource allocation policies

(d) Maximization of the minimum secrecy rate through the optimization of the RIS reflection matrix $\boldsymbol{\Gamma}_R$, the transmit beamforming $\{\boldsymbol{w}_k\}_{k=1}^K$, and artificial noise covariance matrix $\boldsymbol{C}_z$. In this case, no RHS is considered, and the BS is assumed to have an array with $M = 32$ digital antennas, while the RIS is equipped with $N_R = 64$ reflecting elements. The maximization has been performed by specializing Algorithm 5 for minimum secrecy rate maximization, and skipping the subroutine for the optimization of $\boldsymbol{\Gamma}_t$.

(e) Maximization of the minimum SEE through the optimization of the transmit beamforming $\{\boldsymbol{w}_k\}_{k=1}^K$ and artificial noise covariance matrix $\boldsymbol{C}_z$. In this case, no RHS and no RIS are considered, and the BS is assumed to have an array with $M = 32$ digital antennas. The maximization has been performed by Algorithm 5, by skipping the subroutines for the optimization of $\boldsymbol{\Gamma}_t$ and $\boldsymbol{\Gamma}_r$.

(f) Maximization of the minimum secrecy rate through the optimization of the transmit beamforming $\{\boldsymbol{w}_k\}_{k=1}^K$ and artificial noise covariance matrix $\boldsymbol{C}_z$. In this case, no RHS and no RIS are considered, and the BS is assumed to have an array with $M = 32$ digital antennas. The maximization has been performed by specializing Algorithm 5 for minimum secrecy rate maximization, and skipping the subroutines for the optimization of $\boldsymbol{\Gamma}_t$ and $\boldsymbol{\Gamma}_r$.

The results indicate that using an RHS at the base station allows reducing the number of digital antennas that are used, leading to higher SEE levels. Moreover, this is true also if an RIS is deployed in the environment between the transmitter and receiver, in addition to a large antenna array at the BS. Moreover, it is observed that the solutions that aim at secrecy rate maximization lead to a decrease of the SEE level as $P_{\max}$ increases. This happens because the SEE is a unimodal function which admits a finite maximum, and which tends to zero for large transmit powers. Therefore, as $P_{\max}$ becomes large enough to allow attaining the maximum of the SEE, further increasing

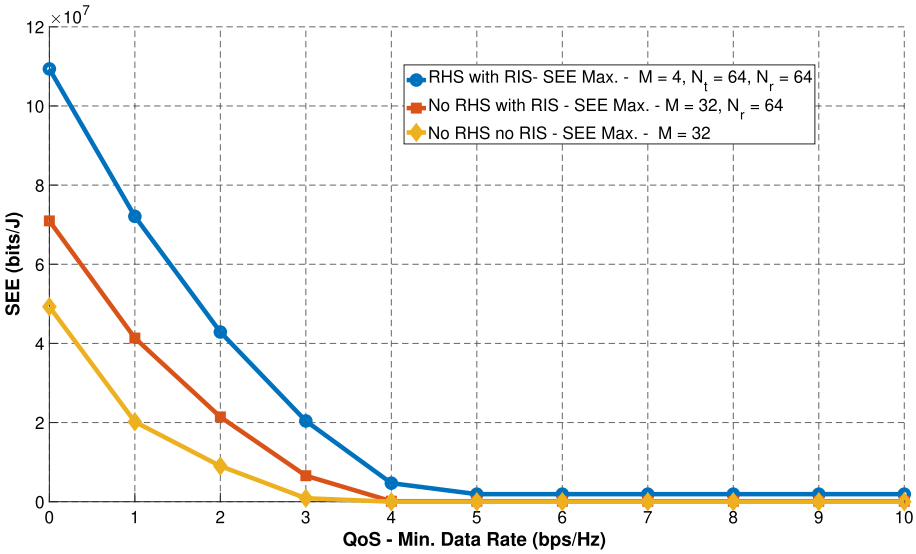

Fig. 3 Minimum SEE versus QoS requirement for different resource allocation policies

the transmit power, as the resource allocation policies that optimize the secrecy rate do, leads to a decrease of the SEE. For the same reason, the resource allocation policies that maximize the SEE tend to saturate for large $P_{\max}$.

Figure 3 shows the achieved minimum SEE versus the QoS constraint $R_{\min} = R_{\min,k}$ for all $k = 1, \ldots, K$, assuming $P_{\max} = 40$ dBm, for the scenarios of Fig. 2 that consider SEE maximization, i.e. cases (a), (c), and (e). The results show again that the best performance is obtained when the BS is equipped with few digital antennas and an RHS is used to increase the array gain of the communication. Besides, the use of the RIS further improves the SEE. Instead, removing the RHS leads to a decrease of the SEE value, even if the size of the transmit array is increased and the RIS is still placed in the propagation environment. It is also seen that the minimum SEE tends to zero as $R_{\min}$ increases. This happens because, for larger $R_{\min}$ values, the problem tends to become unfeasible. If, during the optimization algorithm an unfeasibility is detected, the last feasible solution is considered and the algorithm stops.

Figure 4 analyzes the convergence speed of the proposed Algorithm 5 for minimum SEE maximization, in terms of the number of iterations required to reach convergence, with $R_{\min} = 0$. Cases (a), (c), and (e) from Fig. 2 are considered, and for each of those, the convergence for $P_{\max} = -30$ dBm and $P_{\max} = 0$ dBm has been evaluated. For each optimization policy, Fig. 4 shows the overall iteration count, i.e. considering also the iterations performed to run the algorithms inside the loop of Algorithm 5. This means that the scenario in which also the RHS and RIS matrices are optimized, consider also the iterations required to run the SFP algorithm for the optimization of $\boldsymbol{\Gamma}_t$ and $\boldsymbol{\Gamma}_r$. It is seen that, in all scenarios, convergence is reached fast, except for the case in which both RHS and RIS are optimized and $P_{\max} = 0$ dBm. Nevertheless, even in this case, the minimum SEE value stabilizes after 30 iterations, which include the iterations of the outer alternating optimization, as well as the SFP algorithm for both $\boldsymbol{\Gamma}_t$ and $\boldsymbol{\Gamma}_r$, and the generalized Dinkelbach's method for $\{\boldsymbol{w}_k\}_{k=1}^K$ and $\boldsymbol{C}_z$.

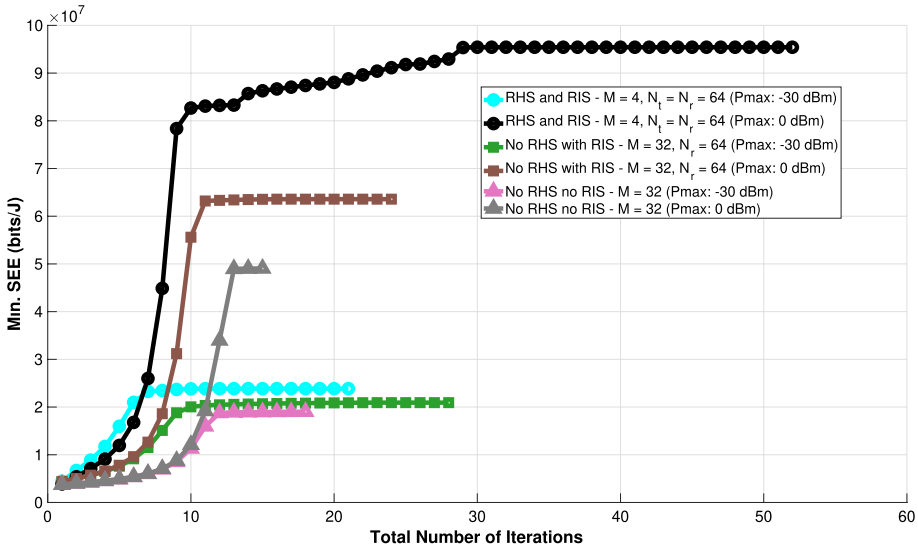

Fig. 4 Minimum SEE versus convergence iterations for different resource allocation policies

Finally, Fig. 5 assumes $N_t = N_R = 32$, $P_{max} = 30\,\text{dBm}$, while the other parameters are as in Fig. 2. In this scenario, the minimum SEE provided by Algorithm 5 is shown versus the number of outer iterations of Algorithm 5, for the following eight initialization strategies:

- $\boldsymbol{\Gamma}_T$ and $\boldsymbol{\Gamma}_R$ initialized with phases randomly selected in $[0, 2\pi]$, beamforming vectors $\boldsymbol{w}_1, \ldots, \boldsymbol{w}_K$ initialized to maximum transmit combining, and the covariance matrix $\boldsymbol{C}_z$ of the artificial noise initialized to a scaled identity matrix such that $\sum_{k=1}^{K} \|\mathbf{w}_k\|^2 + \text{Tr}(\mathbf{C}_z) = P_{\text{max}}$. This initialization is labeled *Random RHS/RIS, MRT, Isotropic AN* in Fig. 5.
- $\boldsymbol{\Gamma}_T$ and $\boldsymbol{\Gamma}_R$ initialized with phases randomly selected in $[0, 2\pi]$; beamforming vectors $\boldsymbol{w}_1, \ldots, \boldsymbol{w}_K$ initialized to maximum transmit combining; the covariance matrix $\boldsymbol{C}_z$ of the artificial noise chosen such that its columns span the null space of $\boldsymbol{W} = [\boldsymbol{w}_1, \ldots, \boldsymbol{w}_K]$. This initialization is labeled *Random RHS/RIS, MRT, Null space AN* in Fig. 5.
- $\boldsymbol{\Gamma}_T$ and $\boldsymbol{\Gamma}_R$ initialized with phases randomly selected in $[0, 2\pi]$; beamforming vectors $\boldsymbol{w}_1, \ldots, \boldsymbol{w}_K$ initialized according to the regularized zero-forcing strategy; the covariance matrix $\boldsymbol{C}_z$ of the artificial noise initialized to a scaled identity matrix such that $\sum_{k=1}^{K} \|\mathbf{w}_k\|^2 + \text{Tr}(\mathbf{C}_z) = P_{\text{max}}$. This initialization is labeled *Random RHS/RIS, RZF, Isotropic AN* in Fig. 5.
- $\boldsymbol{\Gamma}_T$ and $\boldsymbol{\Gamma}_R$ initialized with phases randomly selected in $[0, 2\pi]$; beamforming vectors $\boldsymbol{w}_1, \ldots, \boldsymbol{w}_K$ initialized according to the regularized zero-forcing strategy; the covariance matrix $\boldsymbol{C}_z$ of the artificial noise chosen such that its columns span the null space of $\boldsymbol{W} = [\boldsymbol{w}_1, \ldots, \boldsymbol{w}_K]$; This initialization is labeled *Random RHS/RIS, RZF, Null space AN* in Fig. 5.
- $\boldsymbol{\Gamma}_T$ and $\boldsymbol{\Gamma}_R$ initialized so that the phases of the components of the vector $\text{diag}(\boldsymbol{\Gamma}_T)$ are equal to the phases of the dominant eigenvector of the channel $\boldsymbol{Q}_t$ from the trans-

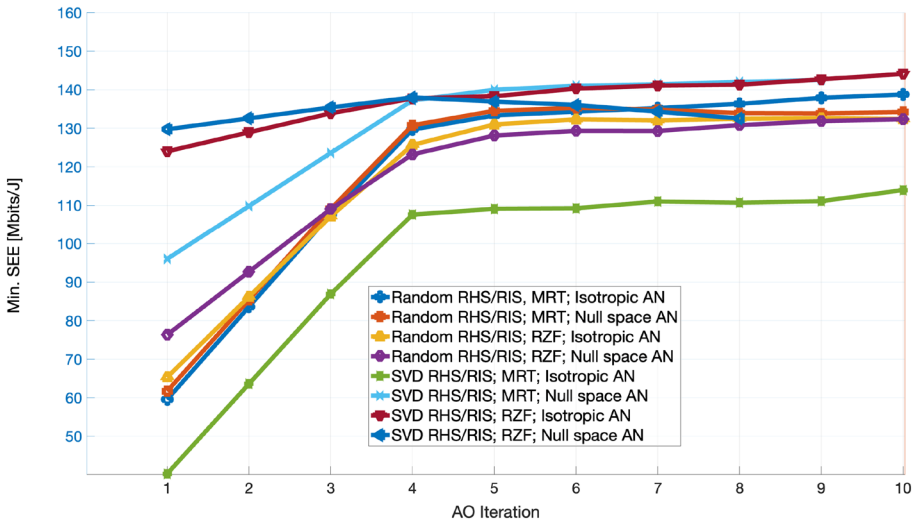

Fig. 5 Minimum SEE for different initialization policies

mitter to the RHS and the phases of the vector $\mathbf{diag}(\boldsymbol{\Gamma}_R)$ are equal to the phases of the dominant eigenvector of the channel $\boldsymbol{Q}_r$ from the RHS to the RIS; beamforming vectors $\boldsymbol{w}_1, \ldots, \boldsymbol{w}_K$ initialized to maximum transmit combining; the covariance matrix $\boldsymbol{C}_z$ of the artificial noise initialized to a scaled identity matrix such that $\sum_{k=1}^{K} \|\mathbf{w}_k\|^2 + \mathrm{Tr}(\mathbf{C}_z) = P_{\max}$; This initialization is labeled *SVD RHS/RIS, MRT, Isotropic AN* in Fig. 5.

- $\boldsymbol{\Gamma}_T$ and $\boldsymbol{\Gamma}_R$ initialized so that the phases of the components of the vector $\mathbf{diag}(\boldsymbol{\Gamma}_T)$ are equal to the phases of the dominant eigenvector of the channel $\boldsymbol{Q}_t$ from the transmitter to the RHS and the phases of the vector $\mathbf{diag}(\boldsymbol{\Gamma}_R)$ are equal to the phases of the dominant eigenvector of the channel $\boldsymbol{Q}_r$ from the RHS to the RIS; beamforming vectors $\boldsymbol{w}_1, \ldots, \boldsymbol{w}_K$ initialized to maximum transmit combining; the covariance matrix $\boldsymbol{C}_z$ of the artificial noise chosen such that its columns span the null space of $\boldsymbol{W} = [\boldsymbol{w}_1, \ldots, \boldsymbol{w}_K]$. This initialization is labeled *SVD RHS/RIS, MRT, Null space AN* in Fig. 5.
- $\boldsymbol{\Gamma}_T$ and $\boldsymbol{\Gamma}_R$ initialized so that the phases of the components of the vector $\mathbf{diag}(\boldsymbol{\Gamma}_T)$ are equal to the phases of the dominant eigenvector of the channel $\boldsymbol{Q}_t$ from the transmitter to the RHS and the phases of the vector $\mathbf{diag}(\boldsymbol{\Gamma}_R)$ are equal to the phases of the dominant eigenvector of the channel $\boldsymbol{Q}_r$ from the RHS to the RIS; beamforming vectors $\boldsymbol{w}_1, \ldots, \boldsymbol{w}_K$ initialized according to the regularized zero-forcing strategy; the covariance matrix $\boldsymbol{C}_z$ of the artificial noise initialized to a scaled identity matrix such that $\sum_{k=1}^{K} \|\mathbf{w}_k\|^2 + \mathrm{Tr}(\mathbf{C}_z) = P_{\max}$; This initialization is labeled *SVD RHS/RIS, RZF, Isotropic AN* in Fig. 5.
- $\boldsymbol{\Gamma}_T$ and $\boldsymbol{\Gamma}_R$ initialized so that the phases of the components of the vector $\mathbf{diag}(\boldsymbol{\Gamma}_T)$ are equal to the phases of the dominant eigenvector of the channel $\boldsymbol{Q}_t$ from the transmitter to the RHS and the phases of the vector $\mathbf{diag}(\boldsymbol{\Gamma}_R)$ are equal to the phases of the dominant eigenvector of the channel $\boldsymbol{Q}_r$ from the RHS to the RIS; beamforming vectors $\boldsymbol{w}_1, \ldots, \boldsymbol{w}_K$ initialized according to the regularized zero-forcing strategy; the covariance matrix $\boldsymbol{C}_z$ of the artificial noise chosen such that

its columns span the null space of $\boldsymbol{W} = [\boldsymbol{w}_1, \ldots, \boldsymbol{w}_K]$. This initialization is labeled *SVD RHS/RIS, RZF, Null space AN* in Fig. 5.

The figure shows that with all initializations the convergence takes place in a few outer iterations of Algorithm 5. The efficiency of the solution upon convergence is also similar, with only the *SVD RHS/RIS, MRT, Isoptropic AN* scheme suffering a clear gap compared to the other algorithms.

5 Conclusion

The problem of secure energy efficiency (SEE) maximization has been addressed in a multi-user multiple-input single-output (MISO) communication system enhanced by an RHS deployed at the transmitter and an RIS placed in the environment between the transmitter and receiver. The presence of a passive eavesdropper and the use of artificial noise has been considered. In this scenario, the problem of maximizing the minimum of the users' SEEs has been tackled by a blend of alternating optimization, generalized fractional programming, and sequential optimization, in order to optimize the reflection coefficients of the two metasurfaces, and the digital beamforming at the transmitter. Numerical results have shown that the proposed algorithms lead to large EE values, and, notably, that the use of the RHS allows reducing the number of digital antennas compared to traditional beamforming techniques, which yields a significant EE improvement. A notable future line of work is the consideration of imperfect channel state information at the transmitter, due to non-negligible errors in the estimation of the propagation channels. This leads to a new optimization problem, which considers the optimization of the worst-case, or the average energy efficiency.

Acknowledgements
Not applicable.

Author contributions
R.F. worked on the numerical simulation and wrote the initial version of the paper. A.I. contributed to the writing of the paper and definition of simulation setup. A.Z. took the lead in the writing of the paper. C.D. contributed to the writing of the paper and final proofreading.

Funding
The work of R. Fotock has received funding from the Project "Garden", funded by EU in NextGeneration EU plan, Mission 4, Component 1, CUP H53D23000480001, through the Italian "Bando Prin 2022 - D.D. 104 del 02-02-2022" by MUR.
The work of A.L. Imoize has received funding from the European Commission through the project HE-DN-INTEGRATE, grant agreement number 101072924.
The work of A.Zappone has been funded by the European Union - NextGenerationEU under the project NRRP RESTART, RESearch and innovation on future Telecommunications systems and networks, to make Italy more smART PE_00000001 - Cascade Call SMART project, with CUP E63C22002040007.

Data availability
The datasets generated and/or analyzed during the current study are available from the corresponding author on reasonable request.

Declarations

Ethics approval and Consent to participate
Not applicable.

Consent for publication
Not applicable.

Competing interests
The authors declare that they have no competing interests.

Received: 3 April 2025 Accepted: 31 May 2025
Published online: 10 July 2025

References

1. M. Di Renzo, F.H. Danufane, X. Xi, J. De Rosny, S. Tretyakov, Analytical modeling of the path-loss for reconfigurable intelligent surfaces–anomalous mirror or scatterer? In: 2020 IEEE 21st International Workshop on Signal Processing Advances in Wireless Communications (SPAWC), pp. 1–5 (2020). IEEE
2. M. Di Renzo, M. Debbah, D.-T. Phan-Huy, A. Zappone et al., Smart radio environments empowered by reconfigurable AI meta-surfaces: an idea whose time has come. EURASIP J. Wirel. Commun. Netw. **2019**, 129 (2019)
3. Q. Wu, R. Zhang, Towards smart and reconfigurable environment: intelligent reflecting surface aided wireless network. IEEE Commun. Mag. **58**(1), 106–112 (2019)
4. C. Huang, G.C. Alexandropoulos, C. Yuen, M. Debbah, Indoor signal focusing with deep learning designed reconfigurable intelligent surfaces. In: 2019 IEEE 20th International Workshop on Signal Processing Advances in Wireless Communications (SPAWC), pp. 1–5 (2019). IEEE
5. Y. Yuan, Y. Huang, X. Su, B. Duan, N. Hu, M. Di Renzo, Reconfigurable intelligent surface (RIS) system level simulations for industry standards. arXiv:2409.13405 (2024)
6. Huawei Technologies: Green 5G building a sustainable world. https://www.huawei.com/en/public-policy/green-5g-building-a-sustainable-world (2020)
7. R. Long, Y.C. Liang, Y. Pei, E.G. Larsson, Active reconfigurable intelligent surface-aided wireless communications. IEEE Trans. Wirel. Commun. **20**(8), 4962–4975 (2021)
8. Z. Zhang et al., Active RIS vs. passive RIS: Which will prevail in 6G? IEEE Trans. Commun. **71**(3), 1707–1725 (2023)
9. R.K. Fotock, A. Zappone, M. Di Renzo, Energy efficiency optimization in RIS-aided wireless networks: active versus nearly-passive RIS with global reflection constraints. IEEE Trans. Commun. (2023). https://doi.org/10.1109/TCOMM.2023.3320700
10. V. Ziegler, P. Schneider, H. Viswanathan, M. Montag, S. Kanugovi, A. Rezaki, Security and trust in the 6G era. Nokia Bell Labs White Pap. **9**, 142314–142327 (2021)
11. K. Norrman, B. Sahlin, B. Smeets, E. Thormarker, E. Fogelström, 6G security – drivers and needs. Ericsson White Pap. (2024)
12. M. Mitev, A. Chortil, H.V. Poor, G.P. Fettweis, What physical layer security can do for 6G security. IEEE Open J. Veh. Technol. **4**, 375–388 (2023)
13. A.B. Kihero, H.M. Furqan, M.M. Sahin, H. Arslan, 6G and beyond wireless channel characteristics for physical layer security: opportunities and challenges. IEEE Wirel. Commun. **31**, 295–301 (2024)
14. A. Chorti, A.N. Barreto, S. Köpsell, M. Zoli, M. Chafii, P. Sehier, G. Fettweis, H.V. Poor, Context-aware security for 6G wireless: the role of physical layer security. IEEE Commun. Stand. Mag. **6**, 102–108 (2022)
15. M.H. Khoshafa, et al. RIS-assisted physical layer security in emerging RF and optical wireless communication systems: a comprehensive survey. arXiv:2403.10412 (2024)
16. A. Zappone, P.H. Lin, E.A. Jorswieck, Energy efficiency of confidential multi-antenna systems with artificial noise and statistical CSI. IEEE J. Sel. Top. Signal Process. **10**(8), 1462–1477 (2016)
17. X. Li, Y. Zheng, M. Zeng, Y. Liu, O.A. Dobre, Enhancing secrecy performance for STAR-RIS NOMA networks. IEEE Trans. Veh. Technol. **72**(2), 2684–2688 (2023). https://doi.org/10.1109/TVT.2022.3213334
18. Y. Pei, X. Yue, W. Yi, Y. Liu, X. Li, Z. Ding, Secrecy outage probability analysis for downlink RIS-NOMA networks with on-off control. IEEE Trans. Veh. Technol. **72**(9), 11772–11786 (2023). https://doi.org/10.1109/TVT.2023.3267531
19. I. Trigui, W. Ajib, W.-P. Zhu, Secrecy outage probability and average rate of RIS-aided communications using quantized phases. IEEE Commun. Lett. **25**(6), 1820–1824 (2021). https://doi.org/10.1109/LCOMM.2021.3057850
20. P. Xu, G. Chen, G. Pan, M. Di Renzo, Ergodic secrecy rate of RIS-assisted communication systems in the presence of discrete phase shifts and multiple eavesdroppers. IEEE Wirel. Commun. Lett. **10**(3), 629–633 (2021). https://doi.org/10.1109/LWC.2020.3044178
21. Z. Zhang, J. Chen, Y. Liu, Q. Wu, B. He, L. Yang, On the secrecy design of STAR-RIS assisted uplink NOMA networks. IEEE Trans. Wirel. Commun. **21**(12), 11207–11221 (2022). https://doi.org/10.1109/TWC.2022.3190563
22. L. Yang, J. Yang, W. Xie, M.O. Hasna, T. Tsiftsis, M. Di Renzo, Secrecy performance analysis of RIS-aided wireless communication systems. IEEE Trans. Veh. Technol. **69**(10), 12296–12300 (2020). https://doi.org/10.1109/TVT.2020.3007521
23. M.-M. Zhao, K. Xu, Y. Cai, Y. Niu, L. Hanzo, Secrecy rate maximization of RIS-assisted swipt systems: a two-timescale beamforming design approach. IEEE Trans. Wirel. Commun. **22**(7), 4489–4504 (2023). https://doi.org/10.1109/TWC.2022.3225969
24. T.M. Hoang, C. Xu, A. Vahid, H.D. Tuan, T.Q. Duong, L. Hanzo, Secrecy-rate optimization of double RIS-aided space-ground networks. IEEE Internet Things J. **10**(15), 13221–13234 (2023). https://doi.org/10.1109/JIOT.2023.3262481
25. Y. Li, Y. Zou, J. Zhu, B. Ning, L. Zhai, H. Hui, Y. Lou, C. Qin, Sum secrecy rate maximization for active RIS-assisted uplink SIMO-NOMA networks. IEEE Commun. Lett. (2023). https://doi.org/10.1109/LCOMM.2023.3323537
26. Y. Chen, Y. Wang, Z. Wang, P. Zhang, Robust beamforming for active reconfigurable intelligent omni-surface in vehicular communications. IEEE J. Sel. Areas Commun. **40**(10), 3086–3103 (2022)
27. Q. Zhu, M. Li, R. Liu, Y. Liu, Q. Liu, Joint beamforming designs for active reconfigurable intelligent surface: a sub-connected array architecture. IEEE Trans. Commun. **70**(11), 7628–7643 (2022)
28. K. Liu, Z. Zhang, L. Dai, S. Xu, F. Yang, Active reconfigurable intelligent surface: fully-connected or sub-connected? IEEE Commun. Lett. **26**(1), 167–171 (2022)
29. Y. Ma, M. Li, Y. Liu, Q. Wu, Q. Liu, Active reconfigurable intelligent surface for energy efficiency in MU-MISO systems. IEEE Trans. Veh. Technol. **72**(3), 4103–4107 (2023)

30. K. Shen, W. Yu, Fractional programming for communication systems–Part I: power control and beamforming. IEEE Trans. Signal Process. **66**(10), 2616–2630 (2018)
31. Q. Peng, Q. Wu, G. Chen, R. Liu, S. Ma, W. Chen, Hybrid active-passive IRS assisted energy-efficient wireless communication. IEEE Commun. Lett. **27**(8), 2202–2206 (2023)
32. Y. Wang et al., Secure satellite transmission with active reconfigurable intelligent surface. IEEE Commun. Lett. **26**(12), 3029–3033 (2022)
33. Y. Zhang, Y. Lu, R. Zhang, B. Ai, D. Niyato, Deep reinforcement learning for secrecy energy efficiency maximization in RIS-assisted networks. IEEE Trans. Veh. Technol. **72**(9), 12413–12418 (2023). https://doi.org/10.1109/TVT.2023.3269805
34. Y. Lu, Secrecy energy efficiency in RIS-assisted networks. IEEE Trans. Veh. Technol. **72**(9), 12419–12424 (2023). https://doi.org/10.1109/TVT.2023.3269905
35. W. Hao, J. Li, G. Sun, C. Huang, M. Zeng, O.A. Dobre, C. Yuen, Max-min security energy efficiency optimization for RIS-aided cell-free networks. 2023 IEEE International Communications Conference (2023)
36. S. Soderi, A. Brighente, S. Xu, M. Conti, Multi-RIS aided VLC physical layer security for 6G wireless networks. IEEE Trans. Mob. Comput. **23**, 15182 (2024)
37. S. Goel, R. Negi, Guaranteeing secrecy using artificial noise. IEEE Trans. Wirel. Commun. **7**(6), 2180–2189 (2008)
38. A. Zappone, E.A. Jorswieck, Energy efficiency in wireless networks via fractional programming theory. Found. Trends® Commun. Inf. Theory **11**(3–4), 185–396 (2015)
39. A. Ben-Tal, A. Nemirovski, Lectures on Modern Convex Optimization. MPS/SIAM Series on Optimization. MPS/SIAM, ??? (2001)
40. V. Degli-Esposti, E.M. Vitucci, M. Di Renzo, S. Tretyakov, Reradiation and scattering from a reconfigurable intelligent surface: a general macroscopic model. IEEE Trans. Antenna Propag. **70**(10), 8691–8706 (2022)
41. C. Feng, H. Lu, Y. Zeng, T. Li, S. Jin, R. Zhang, Near-field modelling and performance analysis for extremely large-scale IRS communications. IEEE Trans. Wirel. Commun. **23**(5), 4976–4989 (2024)

Publisher's Note